Arabian Journal of Chemistry (2022) **15**, 103521

King Saud University

Arabian Journal of Chemistry

www.ksu.edu.sa
www.sciencedirect.com

ORIGINAL ARTICLE

Molecular docking evaluation of celecoxib on the boron nitride nanostructures for alleviation of cardiovascular risk and inflammatory

Yan Cao [a], Malihe Noori [b], Marziyeh Nazari [c,d], Andrew Ng Kay Lup [e,f], Alireza Soltani [b,*], Vahid Erfani-Moghadam [g,*], Aref Salehi [h,*], Mehrdad Aghaei [b,*], Md Lutfor Rahman [i,*], Mohd Sani Sarjadi [i], Shaheen M. Sarkar [j], Chia-Hung Su [k,*]

[a] *School of Mechatronic Engineering, Xi'an Technological University, Xi'an 710021, China*
[b] *Golestan Rheumatology Research Center, Golestan University of Medical Science, Gorgan, Iran*
[c] *Mathematics and Physics Department, School of Engineering, Australian College of Kuwait, Safat, 13015, Kuwait*
[d] *Institute for Sustainable Industries and Liveable Cities (ISILC), Victoria University, Melbourne, VIC, 8001, Australia*
[e] *School of Energy and Chemical Engineering, Xiamen University Malaysia, Jalan Sunsuria, Bandar Sunsuria, 43900 Sepang, Selangor Darul Ehsan, Malaysia*
[f] *College of Chemistry and Chemical Engineering, Xiamen University, Xiamen 361005, Fujian, China*
[g] *Cancer Research Center, Golestan University of Medical Sciences, Gorgan, Iran*
[h] *Ischemic Disorders Research Center, Golestan University of Medical Sciences, Gorgan, Iran*
[i] *Faculty of Science and Natural Resources, Universiti Malaysia Sabah, 88400 Kota Kinabalu, Sabah, Malaysia*
[j] *Department of Applied Science, Technological University of the Shannon, Moylish Park, Limerick V94 EC5T, Ireland*
[k] *Department of Chemical Engineering, Ming Chi University of Technology, New Taipei City, Taiwan*

Received 2 July 2021; accepted 24 October 2021
Available online 29 October 2021

KEYWORDS

BN nanostructures;
Drug delivery;
Anti-inflammatory agents;
Molecular sensor;
DFT

Abstract Celecoxib (CXB) is a nonsteroidal anti-inflammatory drug (NSAID) that can be used to treat rheumatoid arthritis and ischemic heart disease. In this research, density functional theory (DFT) and molecular docking simulations were performed to study the interaction of boron nitride nanotube (BNNT) and boron nitride nanosheet (BNNS) with CXB and its inhibitor effect on pro-inflammatory cytokines. The calculated adsorption energies of CXB with the BNNT were determined in aqueous phase. The results revealed that adsorption of CXB molecule via its SO_2 group on BNNT is thermodynamically favored than the NH_2 and CF_3 groups in the solvent environment. Adsorption of CXB on BN nanomaterials are weak physisorption in nature. This can be attributed

* Corresponding authors.
E-mail addresses: alireza.soltani@goums.ac.ir (A. Soltani), vahiderfani@gmail.com (V. Erfani-Moghadam), salehia@goums.ac.ir (A. Salehi), mehrdadaghaie@yahoo.com (M. Aghaei), lotfor@ums.edu.my (M. Lutfor Rahman), chsu@mail.mcut.edu.tw (C.-H. Su).
Peer review under responsibility of King Saud University.

Production and hosting by Elsevier

https://doi.org/10.1016/j.arabjc.2021.103521

to the fact that both phenyl groups in CXB are not on the same plane and require significant activation energies for conformational changes to obtain greater H-π interaction. Both BNNT and BNNS materials had huge sensitivity in electronic change and short recovery time during CXB interaction, thus having potential as molecular sensor and biomedical carrier for the delivery of CXB drug. IL-1A and TNF-α were implicated as vital cytokines in diverse diseases, and they have been a validated therapeutic target to manage cardiovascular risk in patients with inflammatory bowel disease. A molecular docking simulation confirms that the BNNT loaded CXB could inhibit more pro-inflammatory cytokines including IL-1A and TNF-α receptors as compared to BNNS loaded to CXB.

1. Introduction

In the last decade, boron nitride nanotubes (BNNTs) has been considered for a wide range of applications including nanomedicine, nanoelectronic devices and sensors for biological devices due to their unique surface and physicochemical features (Pakdel et al., 2012; Zhi et al., 2010). Toxicological studies have shown good biocompatibility of BNNTs with various cell lines like pheochromocytoma cells, human neuroblastoma cells, myoblasts (Ciofani et al., 2013) and endothelial cells (Lahiri et al., 2010). Moreover, BNNTs have better biocompatibility than carbon nanotubes as shown by in vivo studies, indicating no adverse effect after the injection in rabbits at a dose up to 10 mg/kg (Ciofani et al., 2013). These properties make BNNTs appropriate for many applications containing nanovectors for biomolecules as DNA (Chen et al., 2009) and for anticancer drugs (Li et al., 2013).

The adsorption of drug molecules onto the BNNTs is a significant subject of interest for drug delivery systems (Bezi Javan et al., 2016; Li et al., 2013; Roosta et al., 2016; Soltani and Baei, 2019; Talla et al., 2019). For example, Shaian and Nowroozi reported the adsorption of 5-fluorouracil on armchair single-walled BNNTs that are of different sizes. They have shown that the encapsulated nanotubes are more stable than the hybrid complexes (Shayan and Nowroozi, 2018). Xu et al. evaluated the non-covalent interactions of BNNTs with carmustine and temozolomide which are brain anticancer drugs by means of density-functional theory methods (Xu et al., 2018). Their results have shown that adsorption of drug molecule within the inner surface of BNNT is stronger due to confinement effect and curvature effect of BNNT tube surface. Theoretical studies on the interaction of BNNT with vitamins (Farmanzadeh and Ghazanfary, 2014), cathinone (Nejati et al., 2017), metformin (Chigo Anota and Cocoletzi, 2014), pyrazinamide (Saikia et al., 2013), hydroxycarbamide (Hesabi and Behjatmanesh-Ardakani, 2017) and amino acids (Singla et al., 2016) have also been reported. These studies would provide a framework for the design of BNNT-based devices for various biomedical applications.

Celecoxib or known as 4-[5-(4-Methylphenyl)-3-(trifluoromethyl) pyrazol-1-yl] benzene sulfonamide) is a 1,3,5-trisubstituted pyrazole or nitrogen-containing heterocyclic compound. CXB can be synthesized via the regioselective 1,3-dipolar cycloaddition reaction between nitrile imine and enamine where the former is formed in situ from hydrazonoyl benzenesulphonate (Oh, 2006). Pyrazoles are commonly known for their anti-viral, anti-parasitic, antibacterial, anti-tumor, anti-fungal and insecticidal activities, thus making them to have extensive biological applications (Emamian, 2015). Among the pyrazoles, CXB is a nonsteroidal anti-inflammatory drug (NSAID) that suppresses inflammation by blocking prostaglandins (PGs) formation as one of the major undesired effects of PGs is their inflammatory response. This is done by inhibiting cyclooxygenase which is the enzyme for PGs biosynthesis.

In the past, cyclooxygenase (COX) was thought to be the single enzyme present in most cells in single isoform, leading to the belief that its inhibition in the event of inflammation suppression would also adversely affect prostaglandin-regulated processes. It was only in the later studies where COX was found to be present in two isoforms: COX-1 and COX-2, to produce prostaglandins (PGs) via cyclooxygenation of arachidonic acid. COX-1 is the constitutive form which produces PGs that are physiologically necessary and commonly found in gastrointestinal tract and kidney tissues. COX-2, on the other hand, is the inducible form that is produced by inflammatory cytokines and endotoxins in the event of inflammation. However, recent studies have also shown the possibility of COX-2 synthesis under non-pathological circumstances (Alaaeddine et al., 2021; Zhang et al., 2021).

Traditional NSAIDs were shown to possess anti-inflammatory activities by inhibiting both COXs at higher COX-1 inhibition selectivity whereas CXB was shown to possess higher inhibition selectivity for COX-2 than COX-1 by 375 fold (Penning et al., 1997). This enabled CXB to produce anti-inflammatory activity with lesser gastrointestinal side effects (Clemett and Goa, 2000). This preferential COX inhibition has been investigated by Price and Jorgensen (Price and Jorgensen, 2001). Their study showed that both COXs have different residue identities at position 523 which affect the binding of sulfonamide moiety in CXB. Isoleucine (Ile523) occupies position 523 in COX-1 whereas valine (Val523) occupies position 523 in COX-2. Steric effect between sulfonamide oxygen of CXB and δ methyl group of Ile523 in COX-1 was prominent, thus reducing CXB affinity for COX-1.

CXB is presently endorsed by the Food and Drug Administration (FDA) for symptomatic treatment of adult osteoarthritis (OA) and adult rheumatoid arthritis (RA) (Chawla et al., 2003; Lee and Lee, 2013; Abdolahi et al., 2018; Hezarkhani et al., 2014; Roshande et al., 2018). Studies on the use of CXB as novel anticancer drug for colorectal cancer were also undertaken where inhibition of polyp growth were observed (Schönthal et al., 2008; Zhu et al., 2002). However, further studies and clinical trials are required as the mechanism and the side effects of CXB based cancer treatments are yet to be accurately established (Half and Arber, 2009). The administration of celecoxib drug in its pristine and unassisted form is challenging as it crystallizes easily (Gupta et al., 2004). Thus, the use of biomedical carrier is necessary to improve its dispersion and solubility in protic environment for effective drug release (Xue et al., 2021; Li and Wang, 2021; Li et al., 2020; Zhang et al., 2016; He et al., 2021; Zhang et al., 2020; Hu et al., 2021). Previous theoretical study on effective CXB drug transport using $B_{12}N_{12}$ fullerene has been reported (Abdolahi et al., 2018).

Suitable adsorbent features of BN nanostructures have been validated for targeted delivery of anti-inflammatory and anticancer drugs in various experimental and theoretical studies (Zhang et al., 2012; Feng et al., 2016; Feng et al., 2018; Khalifi et al., 2015; Duverger and Picaud, 2020; Duverger et al., 2019; Duverger et al., 2017; Mlaouah et al., 2018; El Khalifi et al., 2016; Palomino-Asencio et al., 2021; Chigo Anota et al., 2017; Muñoz et al., 2021; Anota et al., 2015; Escobedo-Morales et al., 2019). To the best knowledge of authors, the interaction of BN nanostructures with celecoxib has yet to be investigated. Thus, herein this work, we conducted a systematic theoretical study on the interactions of an isolated celecoxib molecule with the *zigzag* (8,0) single-walled BN nanotube (SWBNNT) and

the BN nanosheet (BNNS). Molecular docking studies were also carried out to investigate the interaction of CXB-BN complexes with protein structures for applications involving cardiovascular risk management in patients with inflammatory bowel disease.

2. Computational methods

The relaxed geometries of (8,0) *zigzag* BNNT, BNNS, CXB and their adsorption complexes of different orientations were fully optimized and then evaluated by DFT study. The DFT method used was Perdew-Burke-Ernzerhof (PBE) functional which is a version of Grimme's D dispersion model with 6-311G** basis set level of theory (Perdew et al., 1996). The hybrid PBE-D functional is suitable for applications involving nanoscale molecular systems. Additionally, PBE-D functional has good reliability in computing binding energies of organic molecules on (8,0) *zigzag* BNNT (Alinezhad et al., 2017; Saikia and Deka, 2014; Soltani et al., 2014; Baei et al., 2014; Srimathi et al., 2018; Srimathi et al., 2018). Solvent effects were studied through using polarizable continuum model (PCM) with water (dielectric constant of 78.4) as the solvent. CXB interaction in aqueous environment was investigated to determine the properties of the CXB/BNNT system for effective mediation of therapeutics by nanotubes within the body (Sukhorukova et al., 2015; Ghahremani et al., 2019; Permyakova et al., 2017). The convergence criteria for geometry relaxation are 0.00045/0.0003 a.u. and 0.0018/0.0012 a.u. for the maximum and root-mean-square forces and the maximum and root-mean-square displacements, respectively. The spin multiplicity of the structures was set to one with relevance to its ground state molecular orbital (its ground electronic state is $^1\Sigma^+$). In addition, frontier molecular orbital (FMO) and density of states (DOS) have also been undertaken to study other important features of the computed systems. Computational studies were performed using DFT formalism implemented in Gaussian 09 package (Frisch et al., 2009). Vibrational frequencies were also calculated at PBE functional with 6-311G** basis set.

We evaluated the effect of BSSE (basis set superposition error) correction using counter poise correction method in the computations of week intermolecular interactions by approximating the BSSE energy. All the calculations were undertaken at T = 298.15 K. The adsorption energy (E_{ads}) of CXB on the pristine BNNT was determined by (Equation (1)):

$$E_{ads} = E_{BNNT-CXB} - (E_{BNNT} + E_{CXB}) + E_{BSSE} \quad (1)$$

where E_{BNNT} is the total energy of the pristine BNNT. $E_{BNNT-CXB}$ is the total energy of CXB adsorbed onto the pristine BNNT and E_{CXB} represents the total energy of an isolated CXB drug. Physical and chemical properties of BNNT, BNNS and adsorption complexes were analyzed using quantum molecular descriptors (Hoseininezhad-Namin et al., 2020; Soltani et al., 2017): chemical potential (μ), electronegativity (χ), global hardness (η), global softness (S) and electrophilicity index (ω). Koopmans' approximation was used for the computation of quantum molecular descriptors where ionization potential and electron affinity were respectively approximated as the negative of HOMO and LUMO energies.

Auto Dock software package (4.2) was used for molecular docking studies (Morris et al., 2009) where TNF-alpha (PDB ID: 2AZ5) and IL1A-S100A13 complex (PDB ID: 2L5X) were selected as sample crystal structures from Protein Data Bank. The protein structures were prepared with the procedure of cognate ligand removal, hydrogen atoms addition, non-polar hydrogen merging and Kollman charge allocation using Auto Dock Tools (ADT). Local search method of Lamarckian genetic algorithm was used in this study. Grid map of 60 × 60 × 60 with 0.375 Å grid spacing was determined for the modeling of the autogrid (Cao et al., 2021; Pavase et al., 2018). 100 GA runs were done for docking. 2D and 3D presentations of the structures were prepared using Maestro 11.0 Schrodinger program.

3. Results and discussion

3.1. Structural analysis of CXB, BNNT and BNNS

The optimized molecular structures of CXB (Fig. 1), (8,0) *zigzag* single-walled BNNT (Fig. 2) and BNNS (Fig. 5) were evaluated by the PBE functional in aqueous phase. For pristine CXB molecule, the bond lengths of C_2-S_1, S_1-O_{25}, S_1-N_{24} and N_8-N_{23} were computed to be 1.783, 1.480, 1.704 and 1.424 Å respectively. Similarly, O_{25}-S_1-O_{26}, C_2-S_1-N_{24}, C_5-N_8-N_{23}, N_8-C_9-C_{10} and F_{22}-C_{19}-F_{21} bond angles of CXB were found to be 122.1°, 103.5°, 117.5°, 125.5° and 108.2° respectively. These observations remain in good agreement with the earlier reported literatures (Vijayakumar et al., 2016; Gundersen and Rankin, 1983). In a theoretical study, C_4-N_{11}-C_{15}, C_{14}-C_{13}-C_{16} and N_{11}-C_{15}-C_{20} bond angles for the CXB molecule were calculated to be 129.64°, 127.97° and 124.78° by B3LYP/6-311G** level of theory (Gundersen and Rankin, 1983).

In this investigation, (8,0) *zigzag* single-walled BNNT and BNNS with the respective dimensions of 6.42 Å diameter and 19 Å length; 6.42 Å width and 19 Å length were used. The structural evaluation of BNNT shows two particular B-N bonds: one parallel to the tube axis and the other skewed with respective bond lengths of 1.454 and 1.460 Å by PBE-D functional. These calculated B-N bond lengths are comparable with the experimental value of 1.446 Å (Pease, 1952). Similarly, BNNS has a B-N bond length of 1.455 Å. The calculated energy gaps, HOMO and LUMO energies of (8,0) *zigzag* BNNT and BNNS were 3.37, −5.52 and −2.15 eV; 3.98,

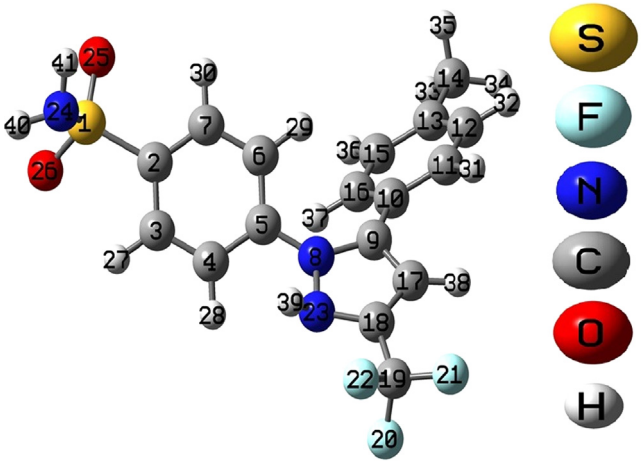

Fig. 1 Optimized molecular structure of celecoxib.

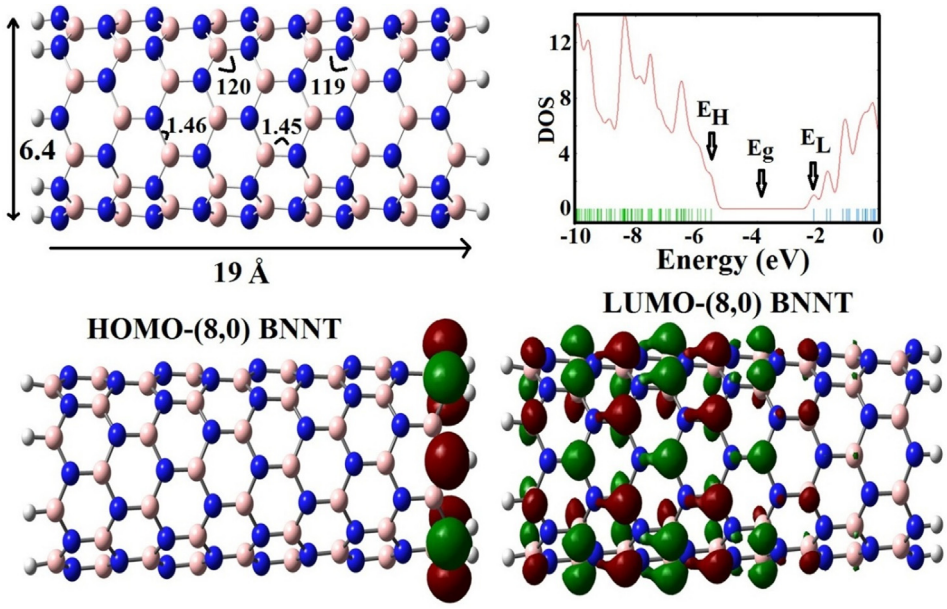

Fig. 2 Optimized molecular structure, FMO and TDOS plots of (8,0) *zigzag* BNNT.

−5.39 and −1.41 eV, respectively. FMO plot of (8,0) *zigzag* BNNT shows the HOMO and LUMO to be on both opposite ends of the tube respectively with the HOMO aligned perpendicularly to the surface of BNNT.

The curved surface of BNNT creates confinement effect where molecular orbitals are closer in proximity such that greater extent of state degeneracy was predicted and observed in the TDOS plot of BNNT. The state degeneracy was more prominent in the upper empty molecular orbitals causing a greater reduction in LUMO energy as compared with that of HOMO energy. HOMO energy is the highest energy level for the ground state of valence electron within the molecule whereas LUMO energy is the lowest energy level for the excited state of valence electron to be achieved. Against this backdrop, the HOMO-LUMO energy gap of BNNT is smaller as compared with that of BNNS which does not experience confinement effect. These would also imply that the BNNT has larger population of conduction electron for better electrical conductivity and adsorption sensitivity.

3.2. Adsorption of CXB on BNNT and BNNS

Adsorption of celecoxib on (8,0) *zigzag* BNNT occurred through its CF_3, SO_2 and NH_2 groups to form three adsorption configurations: CF_3-CXB/BNNT (Model A), SO_2-CXB/BNNT (Model B) and NH_2-CXB/BNNT (Model C) as shown in Fig. 3. Adsorption of celecoxib on BNNS was noted to feasibly occur via its NH_2 group to form NH_2-CXB/BNNS complex (Model G) as shown in Fig. 4. Based on Table 1, the calculated adsorption energies were negative in values indicating CXB adsorption on BNNT and BNNS to be thermodynamically favored. The results revealed that adsorption of CXB molecule via its SO_2 group on BNNT is thermodynamically favored than the NH_2 and CF_3 groups in the solvent environment. However, such adsorptions are generally weak electrostatic interaction (Saikia and Pandey, 2018) as the adsorption energies range between −0.07 eV and −0.15 eV, indicating their physisorptive nature.

During adsorption, B-N bond lengths of BNNT and BNNS were slightly increased which indicate the weakening of B-N bond and its partial bond sharing with the celecoxib groups. The adsorption process involved the sharing of lone pair electrons of F, O or N of celecoxib with the unhybridized empty *p* orbital of boron in BNNT and BNNS depending on the adsorption configuration of celecoxib. This phenomenon is in corroboration with the established role of boron as Lewis acid site in boron nitride materials during molecular interactions (Soltani et al., 2020). Interactions of drug molecules with boron nitride surfaces were also reported to occur via H-π and π-π interactions (Li and Golberg, 2016; Gao et al., 2011). H-π interaction is due to the interaction between hydrogen atoms of celecoxib alkyl groups with boron nitride surface whereas π-π interaction is due to the interaction between the celecoxib rings and the aromatic rings of boron nitride surface.

(8,0) *zigzag* BNNT had slightly larger binding energies than BNNS during their interactions with CXB. As the celecoxib molecule has curvature structure, it can interact better with the curved surface of BNNT due to lower steric repulsion and higher interaction area for H-π and π-π interactions. The optimized CXB molecular structure shows both of the benzene rings in Ph-CH_3 and Ph-SO_2NH_2 groups are not on the same plane. This had cause a lesser extent of π-π interaction which may account for the low adsorption energies of CXB-BNNT complexes. Likewise, Grzybowska *et al.* have also shown that the conformational changes of CXB require significant activation energies which would reduce its interaction extent on BNNT (Grzybowska et al., 2012). To conform both benzene rings in Ph-CH_3 and Ph-SO_2NH_2 groups to be on the same plane, the rotations of Ph-CH_3 and Ph-SO_2NH_2 groups require activations energies of 17 kJ/mol and 16 kJ/mol respectively. In this study, the interaction of CXB was done on the outer surface of BNNT. By interacting CXB with the inner

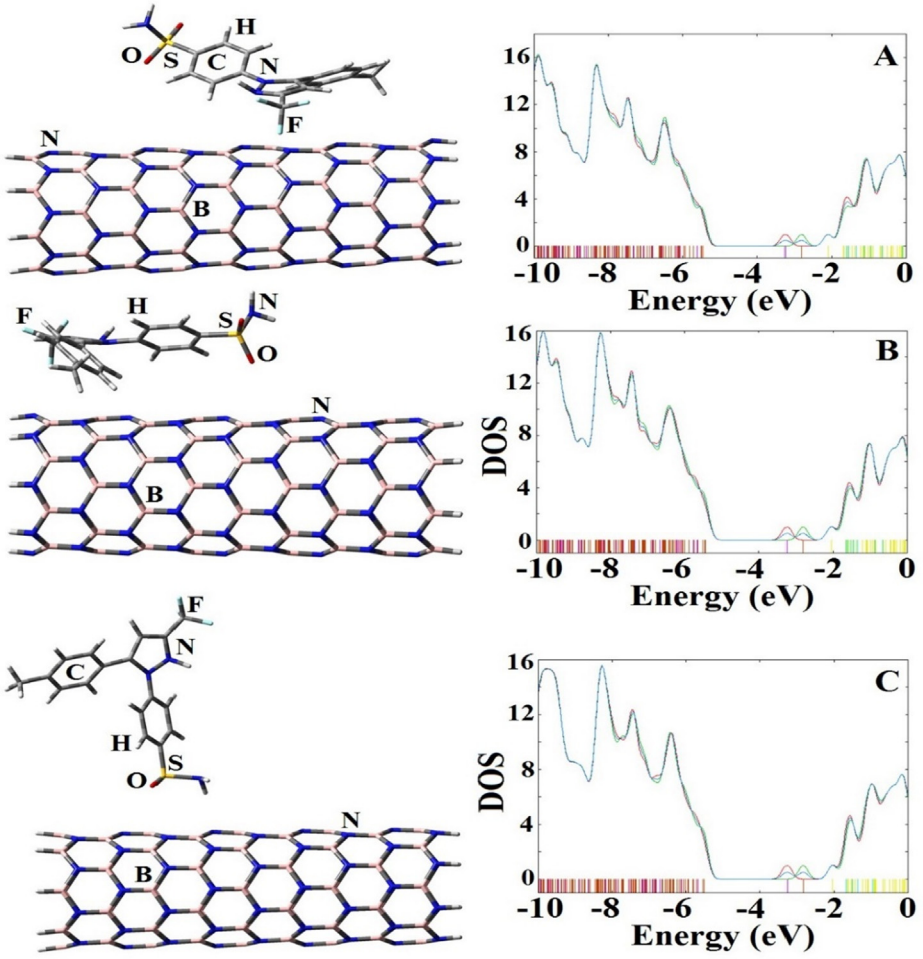

Fig. 3 Geometries and TDOS plots of CF_3-CXB/BNNT (Model A), SO_2-CXB/BNNT (Model B) and NH_2-CXB/BNNT (Model C) adsorption complexes.

surface of BNNT, one could possibly predict a larger adsorption energy though it is physically not possible to be inserted within the BNNT owing to its larger size (1.1 nm × 0.5 nm × 0.9 nm). The aforementioned confinement effect of BNNT would cause the π-orbitals of BNNT at the inner surface to be closer in proximity such that a larger π-π stack interaction with the drug molecule is made possible (Fig. 5) (Xu et al., 2018). Similar trends were also reported by Qian and Fang in their theoretical investigations on the interaction of carmustine and temozolomide drug molecules within BNNT (Qian et al., 2013; Fang et al., 2015). The infrared (IR) spectra of CXB in the states A, B, and C exhibited characteristic bands at 3315, 3326, and 3347 cm^{-1} assign to the N-H stretching vibration of the SO_2NH_2 group, respectively. The characteristic bands observed at 1354, 1334, and 1363 cm^{-1} for the S═O asymmetric and 1162, 1175, and 1186 cm^{-1} for the S═O symmetric stretching vibrations. The C─H stretching vibrations of the CXB in the states A, B, and C observed in the region 3180–3020 cm^{-1} in the heterocyclic aromatic moiety.

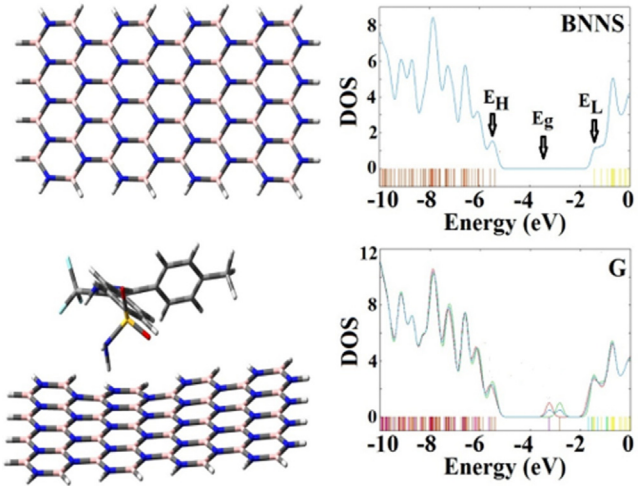

Fig. 4 Geometries and TDOS plots of BNNS and NH_2-CXB/BNNS adsorption complex.

Hybridizations of interacting B atoms in BNNT and BNNS were observed during their interactions with CXB. When B atom forms an additional partial bond with the drug molecule, its orbital hybridization tends to be between sp^2 to sp^3 configuration range. The closer its hybridization to sp^3 configuration, the stronger is the bond. The neutral bond orbital (NBO) analysis by Nejati et al. have shown that the interacting B atom in BN nanocage, nanotube and nanosheet with cathinone molecule were of $sp^{2.78}$, $sp^{2.32}$ and $sp^{2.18}$ respectively (Nejati et al.,

Table 1 Calculated adsorption energies (E_{ads}), B-N and S-O bond lengths, bond distances between CXB and drug carrier (D), HOMO energies (E_H), LUMO energies (E_L), HOMO-LUMO energy gap (E_g), Fermi energy levels (E_F) and dipole moments (μ_D) for CXB/BNNT and CXB/BNNS adsorption complexes.

	E_{ads} (eV)	D (Å)	B-N (Å)	S-O (Å)	E_H (eV)	E_L (eV)	E_g (eV)	ΔE_g (%)	E_F (eV)	μ_D (Debye)
BNNT	−35.9	–	1.454	–	−5.52	−2.15	3.37	–	−3.84	12.57
Model A	−0.11	2.94	1.460	1.482	−3.25	−2.11	1.10	67.36	−2.70	14.79
Model B	−0.15	3.15	1.462	1.485	−3.24	−2.05	1.19	64.69	−2.65	15.19
Model C	−0.08	2.43	1.467	1.483	−3.27	−2.05	1.22	63.80	−2.66	13.14
BNNS	−30.0	–	1.455	–	−5.39	−1.41	3.98	–	−3.40	0.85
Model G	−0.07	2.57	1.457	1.489	−3.24	−1.68	1.56	60.80	−2.46	5.80

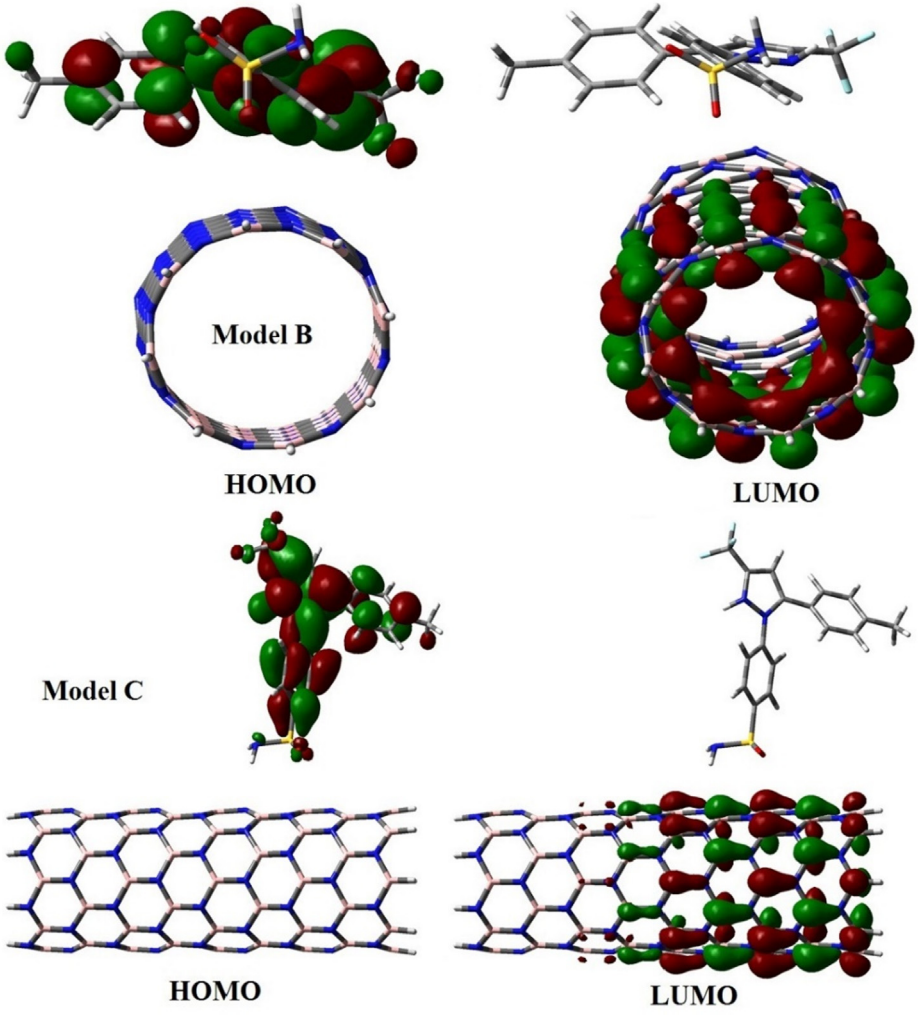

Fig. 5 FMO plots of SO_2-CXB/BNNT (Model B) and NH_2-CXB/BNNT (Model C) adsorption complexes.

2017). Hence, the result in this work corroborates with the aforementioned NBO analysis where interaction of BNNT with CXB is stronger as compared with BNNS as the former has a higher *p* character in its sp^x-hybridization. Hybridization has also resulted additional degenerate states in interacting B atoms as shown in TDOS plots of Fig. 3. These states produced HOMO of higher energy and LUMO of lower energy thus reducing the HOMO-LUMO energy gap in the adsorption complexes.

All adsorption complexes experienced significant HOMO-LUMO energy gap reduction with their energy gap reductions in descending order of: NH_2-CXB/BNNS (2.42 eV) > CF_3-CXB/BNNT (2.27 eV) > SO_2-CXB/BNNT (2.18 eV) > NH_2-CXB/BNNT (2.15 eV). These significant energy gap reductions indicate a significant change in the electronic conductivity of BN nanomaterials during CXB interaction, which could be leveraged for molecular sensor application. Since the conduction electron population, *N* is dependent on the HOMO-

LUMO energy gap, E_g of a material (Equation (2)), the change in conduction electron population due to adsorption could also be determined based on the change in energy gap (Equation (3)) (Amirkhani et al., 2018):

$$N = AT^{3/2}exp\left(-\frac{E_g}{2kT}\right) \quad (2)$$

$$\frac{N_f}{N_i} = exp\left(-\frac{\Delta E_g}{2kT}\right) \quad (3)$$

where A is exponential factor, f and i are pristine material and adsorption complex, ΔE_g is change in HOMO-LUMO energy gap, k is Boltzmann constant, T is absolute temperature. At 298.15 K, CF_3-CXB/BNNT, SO_2-CXB/BNNT, NH_2-CXB/BNNT and NH_2-CXB/BNNS adsorption complexes respectively showed an increase in N_f by 1.53×10^{19}, 2.66×10^{18}, 1.48×10^{18} and 2.84×10^{20} times of N_i. Owing to its larger energy gap reduction, BNNS is more sensitive toward CXB interaction as compared with that of BNNT.

CXB desorption from BN nanomaterials after interaction is important in assessing its recovery performance as molecular sensor or its drug release efficiency. The recovery of BN nanomaterials could be performed via heating or UV light exposure. Based on transition theory, recovery time, τ can be expressed as (Equation (4)) (Vessally et al., 2018):

$$\tau = v^{-1}exp\left(-\frac{E_{ads}}{kT}\right) \quad (4)$$

where v is attempt frequency. Under UV light exposure with an attempt frequency of 10^{15} s^{-1} at 298.15 K, the recovery times for CF_3-CXB/BNNT, SO_2-CXB/BNNT, NH_2-CXB/BNNT and NH_2-CXB/BNNS adsorption complexes are 72.3, 343, 22.5 and 15.3 ns respectively. As the interaction of CXB with BN nanomaterials had low adsorption energies, CXB desorption would be more facile hence enabling easier recovery of BN nanomaterials. These short recovery times in BN nanomaterial can be of interest for molecular sensors involving rapid detection applications (Fang et al., 2015).

Quantum molecular descriptors of CXB molecule were calculated by Vijayakumar et al. using B3LYP/6–311 + + G(d,p) method (Vijayakumar et al., 2016). The reported values of μ and ω were low, indicating that CXB molecule acts as nucleophile during its interaction. This is in corroboration with the partial electron sharing from CXB to BN nanomaterial during adsorption. Upon CXB interaction, the adsorption complexes were predicted to be more reactive as shown by the significant decrease in global hardness (Table 2). The decrease in chemical potential of complexes indicates their better stability and the spontaneity of the interaction. The ω is a size of electrophilic power of a molecule. Higher ω denotes higher electrophilicity of a given system (Parr and Yang, 1989; Parr et al., 1999). The values of ω increased from 4.36 to 2.90 eV in the pure BNNT and BNNS to 6.30 in model **A** and 3.88 eV in model **G**. The ω and χ values were noted to decrease after CXB adsorption, showing a decrement in the reactivity of structures or it could be expounded as the adsorption system reaching a more stable state in resisting chemical changes (Ocotitl Muñoz et al., 2021).

3.3. Molecular docking

The binding affinity of the studied complexes toward tumor necrosis factor-α (TNF-α) and interleukin-1 (IL-1) receptor targets was determined using the AutoDock (4.2) software. To study the inhibition mechanism of TNF-α receptor, the chosen models (**A**, **B**, and **G**) were docked in the binding pocket of TNF-α receptor protein (PDB ID: 2AZ5). Results from docking calculations illustrated that SO_2-CXB/BNNT (Model **B**) is a potent inhibitor of TNF-α as compared with other complexes. The calculated binding energies of the CF_3-CXB/BNNT (Model **A**), SO_2-CXB/BNNT (Model **B**), and SO_2-CXB/BNNS (Model **G**) in the binding pocket of the TNF-α receptor were −8.1, −9.5, and −7.8 kcal/mol respectively (Table 3). Model **B** was stabilized in the binding pocket of TNF-α receptor by hydrophobic interactions by several amino acid residues like Leu142, Pro139, Phe144, Ala22, Pro20, and Ala145 in chain C. Model **B** was also bounded with Lys65, Gln67, Glu23, Asp140, Gln21, and Gly24 in chain C via polar interactions. The calculations showed that the Model **B** was bounded with key amino acid residues in the active functional group inhibiting the TNF-α receptor (Xu et al., 2018; Gao et al., 2021) (Fig. 6). Furthermore, the sulfonamide pharmacophore of CXB complex was stabilized in the binding pocket of the receptor by four hydrogen bonds with the residues of protein like Ala22 and Lys65 (Alam et al., 2016). Hydrogen bond lengths were 2.62, 2.40, 2.83 and 2.84 Å respectively.

The calculated binding energies of the Model **A, B,** and **G** in the binding pocket of IL-1A receptor were −7.4, −8.6, and −6.9 kcal/mol, respectively. Model **B** was established in the binding pocket of the target via hydrophobic interactions through several amino acid residues like Ala42, Ala43, Met1, Ile95, Ala35 and Trp139 (Kim et al., 2016; Soltani et al., 2022). Furthermore, the complex was also stabilized in the binding pocket of the receptor by two hydrogen bonds with the amino acid residue (Ala22). Hydrogen bond lengths were 3.88 and 3.85 Å. 3D models binding mode models demonstrate that the Model **B** was entered in the pockets of the IL-1A receptor (Fig. 7). Model **B** had lower binding affinity to the target structure as the docking models show while presenting

Table 2 Calculated quantum molecular descriptors for BNNT, BNNS, CXB/BNNT and CXB/BNNS adsorption complexes.

	I (eV)	A (eV)	η (eV)	μ (eV)	χ (eV)	S (eV^{-1})	ω (eV)
BNNT	5.52	2.15	1.69	−3.84	3.84	0.30	4.36
Model A	3.25	2.11	0.57	−2.68	2.68	0.88	6.30
Model B	3.24	2.05	0.60	−2.65	2.65	0.84	5.88
Model C	3.27	2.05	0.61	−2.66	2.66	0.82	5.80
BNNS	5.39	1.41	1.99	−3.40	3.40	0.25	2.90
Model G	3.24	1.68	0.78	−2.46	2.46	0.64	3.88

Table 3 The calculated parameters for the complexes with TNF-α receptor and IL-1A receptor.

Compound	PDB ID: 2AZ5		PDB ID:2L5X	
	Binding energy (kcal/mol)	Inhibition constant, K_i (μM)	Binding energy (kcal/mol)	Inhibition constant, K_i (μM)
Model A	−8.1	4.9	−7.4	7.5
Model B	−9.5	3.6	−8.6	5.2
Model G	−7.8	7.3	−6.9	10.4

a stronger interaction towards the binding pocket of the target resulting in more effective inhibition of the active site of the protein than the other states. Overall, the hydrophobic and H-bond interactions possibly play a key role in occupation of the binding pocket (Cao et al., 2021; Cao et al., 2021). These results indicate that the Model **B** is possibly a potential inhibitor of the TNF-α and IL-1A receptors at the binding site. Previous reports demonstrated CXB nanoparticles as therapeutically effective anti-inflammatory drug-delivery system in managing cardiovascular risk in patients with inflammatory bowel disease (Haley et al., 2021; Pala et al., 2021; Baccaro Biondi et al., 2020; Moodley, 2008; El-Husseiny et al., 2020). The inhibition constants $K_i(\mu M)$ in Table 3 show the potency of the interaction models as inhibitor. The higher the inhibiting character of the compound is expected with the lower value of K_i (Aghaei et al., 2021). These results show the strength of the inhibiting models as Model **B** > Model **A** > Model **G** which is accurate for both type of calculations.

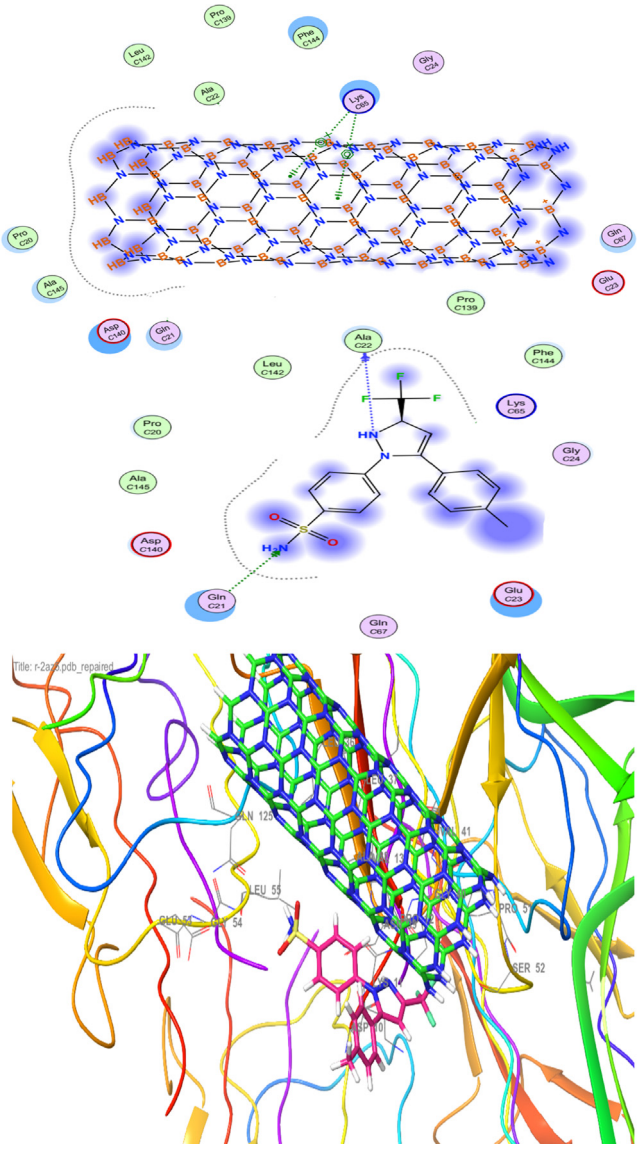

Fig. 6 Docking of 2D and 3D models of interaction between Model B and TNF-α receptor.

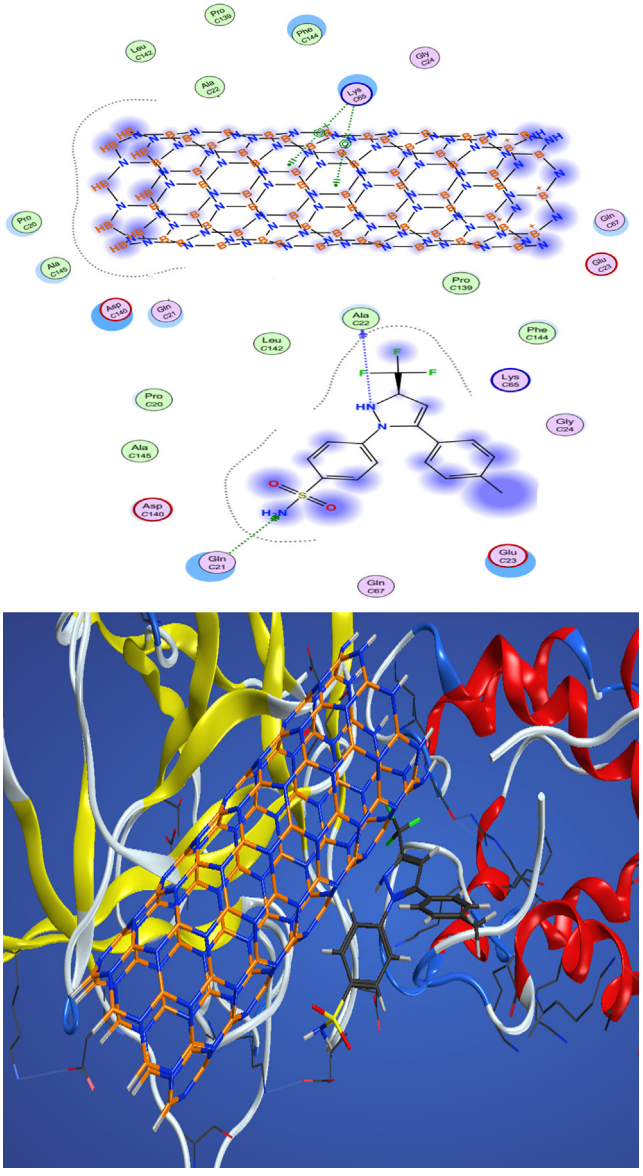

Fig. 7 Docking of 2D and 3D models of interaction between Model B and IL-1 receptor.

4. Conclusions

In this work, by using the DFT/PBE-D functional, theoretical analysis on the geometries and the electronic properties of BNNT and BNNS interacting with CXB drug were done for drug delivery applications. Adsorption of CXB on BN nanomaterials are weak but physisorption in nature. This can be attributed to the fact that both phenyl groups in CXB are not on the same plane and require significant activation energies for conformational changes to obtain greater H-π interaction. Both BNNT and BNNS materials had huge sensitivity in electronic change and short recovery time during CXB interaction, thus having potential for efficient molecular sensor and drug releasing applications. The study of molecular docking showed that the SO_2-CXB/BNNT has a good binding affinity with TNF-α and IL-1A proteins compared to the other studied systems. These calculations could be used to design a novel carrier for the CXB drug delivery system to manage cardiovascular risk in patients with inflammatory bowel disease.

Acknowledgements

We gratefully acknowledge financial support from Golestan University of Medical Science (Ethics Code: IR.GOUMS.REC.1398.218).

References

Abdolahi, N., Aghaei, M., Soltani, A., Azmoodeh, Z., Balakheyli, H., Heidari, F., 2018. Adsorption of celecoxib on B12N12 fullerene: spectroscopic and DFT/TD-DFT study. Spectrochim. Acta A Mol. Biomol. Spectrosc. 204, 348–353.

Aghaei, M., Ramezanitaghartapeh, M., Javan, M., Hoseininezhad-Namin, M.S., Mirzaei, H., Shokuhi Rad, A., Soltani, A., Sedighi, S., Lup, A.N.K., Khori, V., Mahon, P.J., Heidari, F., 2021. Investigations of adsorption behavior and anti-inflammatory activity of glycine functionalized $Al_{12}N_{12}$ and $Al_{12}ON_{11}$ fullerene-like cages. Spectrochim. Acta Part A Mol. Biomol. Spectrosc. 246, 119023.

Alaaeddine, R.A., Elzahhar, P.A., AlZaim, I., Abou-Kheir, W., Belal, A.S.F., El-Yazbi, A.F., 2021. The emerging role of COX-2, 15-LOX and PPARγ in metabolic diseases and cancer: an introduction to novel multi-target directed ligands (MTDLs). Curr. Med. Chem. 28 (11), 2260–2300.

Alam, Md Jahangir, Alam, O., Ahmad Khan, S., Naim, M.J., Islamuddin, M., Singh Deora, G., 2016. Synthesis, anti-inflammatory, analgesic, COX1/2-inhibitory activity, and molecular docking studies of hybrid pyrazole analogues. Drug Des., Dev. Therapy 10, 3529–3543.

Alinezhad, H., Darvish Ganji, M., Soleymani, E., Tajbakhsh, M., 2017. A comprehensive theoretical investigation about the bio-functionalization capability of single walled CNT, BNNT and SiCNT using DNA/RNA nucleobases. Appl. Surf. Sci. 422, 56–72.

Amirkhani, R., Omidi, M.H., Abdollahi, R., Soleymanabadi, H., 2018. Investigation of sarin nerve agent adsorption behavior on BN nanostructures: DFT study. J. Cluster Sci. 29, 757–765.

Anota, E.C., Villanueva, M.S., Toral, D.G., Carrillo, L.T., Melchor Martínez, M.R., 2015. Physicochemical properties of armchair non-stoichiometric Boron Nitride nanotubes: a density functional theory analysis. Superlattices Microstruct. 74, 538–543.

Baccaro Biondi, R., Sidnei Salmazo, P., Zanati Bazan, S.G., Hueb, J. C., Rupp de Paiva, S.A., Sassaki, L.Y., 2020. Cardiovascular risk in individuals with inflammatory bowel disease. Clin. Exp. Gastroenterol. 13, 107–113.

Baei, M.T., Soltani, A., Torabi, P., Hosseini, F., 2014. Formation and electronic structure of C_{20} fullerene transition metal clusters. Monatsh Chem. 145, 1401–1405.

Bezi Javan, M., Soltani, A., Tazikeh Lemeski, E., Ahmadi, A., Moazen Rad, S., 2016. Interaction of $B_{12}N_{12}$ nano-cage with cysteine through various functionalities: a DFT study. Superlattices Microstruct. 100, 24–37.

Cao, Y., Khan, A., Mirzaei, H., Khandoozi, S.R., Javan, M., Ng Kay Lup, A., Norouzi, A., Tazikeh Lemeski, E., Pishnamazi, M., Soltani, A., Albadarin, A.B., 2021. Investigations of adsorption behavior and anti-cancer activity of curcumin on pure and platinum-functionalized B12N12 nanocages. J. Mol. Liq. 334, 116516.

Cao, Y., Khan, A., Balakheyli, H., Ng Kay Lup, A., Ramezani Taghartapeh, M., Mirzaei, H., Khandoozi, S.R., Soltani, A., Aghaei, M., Heidari, F., Sarkar, S.M., Albadarin, A.B., 2021. Penicillamine functionalized B12N12 and B12CaN12 nanocages act as potential inhibitors of proinflammatory cytokines: a combined DFT analysis, ADMET and molecular docking study. Arabian J. Chem. 14, 103200.

Cao, Y., Khan, A., Ghorbani, F., Mirzaei, H., Singla, P., Balakheyli, H., Soltani, A., Aghaei, M., Azmoodeh, Z., Aarabi, M., Tavassoli, S., 2021. Predicting adsorption behavior and anti-inflammatory activity of naproxen interacting with pure boron nitride and boron phosphide fullerene-like cages. J. Mol. Liq. 339, 116678.

Chawla, G., Gupta, P., Thilagavathi, R., Chakraborti, A.K., Bansal, A.K., 2003. Eur. J. Pharm. Sci. 20, 305–317.

Chen, X., Wu, P., Rousseas, M., Okawa, D., Gartner, Z., Zettl, A., Bertozzi, C.R., 2009. Boron nitride nanotubes are noncytotoxic and can be functionalized for interaction with proteins and cells. J. Am. Chem. Soc. 131, 890–891.

Chigo Anota, E., Cocoletzi, G.H., 2014. GGA-based analysis of the metformin adsorption on BN nanotubes. Physica E 56, 134–140.

Chigo Anota, E., Bautista Hernandez, A., Escobedo Morales, A., Castro, M., 2017. Design of the magnetic homonuclear bonds boron nitride nanosheets using DFT methods. J. Mol. Graph. Model. 74, 135–142.

Ciofani, G., Danti, S., Nitti, S., Mazzolaia, B., Mattoli, V., Giorgi, M., 2013. Biocompatibility of boron nitride nanotubes: an up-date of in vivo toxicological investigation. Int. J. Pharm. 444, 85–88.

Ciofani, G., Danti, S., Genchi, G.G., Mazzolai, B., Mattoli, V., 2013. Boron nitride nanotubes: biocompatibility and potential spill-over in nanomedicine. Small 9, 1672–1685.

Clemett, D., Goa, K.L., 2000. A review of its use in osteoarthritis, rheumatoid arthritis and acute pain. Drugs 59 (4), 957–980.

Duverger, E., Picaud, F., 2020. Theoretical study of ciprofloxacin antibiotic trapping on graphene or boron nitride oxide nanoflakes. J. Mol. Model. 26, 135.

Duverger, E., Picaud, F., Stauffer, L., Sonnet, P., 2017. Simulations of graphene nanoflake as a nanovector to improve ZnPc photherapy toxicity; from vacuum to cell membrane. ACS Appl. Mater. Interfaces 43, 37554–37562.

Duverger, E., Balme, S., Bechelany, M., Miele, P., Picaud, F., 2019. Natural payload delivery of the doxorubicin anticancer drug from boron nitride oxide nanosheets. Appl. Surf. Sci. 475, 666–675.

El Khalifi, M., Duverger, E., Gharbi, T., Boulahdoura, H., Picaud, F., 2016. Theoretical use of boron nitride nanotubes as a perfect container for anticancer molecules. Anal. Methods 8, 1367–1372.

El-Husseiny, W.M., El-Sayed, M.A.-A., El-Azab, A.S., AlSaif, N.A., Alanazi, M.M., Abdel-Aziz, A.A.-M., 2020. Synthesis, antitumor activity, and molecular docking study of 2-cyclopentyloxyanisole derivatives: mechanistic study of enzyme inhibition. J. Enzyme Inhib. Med. Chem. 35, 744–758.

Emamian, S., 2015. Understanding the molecular mechanism and regioselectivity in the synthesis of celecoxib via a domino reaction: A DFT study. J. Mol. Graph. Model. 60, 155–161.

Escobedo-Morales, A., Tepech-Carrillo, L., Bautista-Hernández, A., Humberto Camacho-García, J., Cortes-Arriagada, D., Chigo-Anota, E., 2019. Effect of chemical order in the structural stability and physicochemical properties of B12N12 fullerenes. Sci. Rep. 9, 16521.

Fang, C., Wang, K., Stephen, Z.R., Mu, Q., Kievit, F.M., Chiu, D. T., Press, O.W., Zhang, M., 2015. ACS Appl Mater Interface 7, 6674–6682.

Farmanzadeh, D., Ghazanfary, S., 2014. Interaction of vitamins A, B1, C, B3 and D with zigzag and armchair boron nitride nanotubes: a DFT study. C. R. Chim. 17, 985–993.
Feng, S., Zhang, H., Yan, T., Huang, D., Zhi, C., Nakanishi, H., Gao, X.-D., 2016. Folate-conjugated boron nitride nanospheres for targeted delivery of anticancer drugs. Int. J. Nanomed. 11, 4573–4582.
Feng, S., Zhang, H., Zhi, C., Gao, X.-D., Nakanishi, H., 2018. pH-responsive charge-reversal polymerfunctionalized boron nitride nanospheres for intracellular doxorubicin delivery. Int. J. Nanomed. 13, 641–652.
Frisch, M.J., Trucks, G.W., Schlegel, H.B., Scuseria, G.E., Robb, M. A., Cheeseman, J.R., Scalmani, G., Barone, V., Mennucci, B., Petersson, G.A., Nakatsuji, H., Caricato, M., Li, X., Hratchian, H. P., Izmaylov, A.F., Bloino, J., Zheng, G., Sonnenberg, J.L., Hada, M., Ehara, M., Toyota, K., Fukuda, R., Hasegawa, J., Ishida, M., Nakajima, T., Honda, Y., Kitao, O., Nakai, H., Vreven, T., Montgomery Jr., J.A., Peralta, J.E., Ogliaro, F., Bearpark, M., Heyd, J.J., Brothers, E., Kudin, K.N., Staroverov, V.N., Kobayashi, R., Normand, J., Raghavachari, K., Rendell, A., Burant, J.C., Iyengar, S.S., Tomasi, J., Cossi, M., Rega, N., Millam, J.M., Klene, M., Knox, J.E., Cross, J.B., Bakken, V., Adamo, C., Jaramillo, J., Gomperts, R., Stratmann, R.E., Yazyev, O., Austin, A.J., Cammi, R., Pomelli, C., Ochterski, J.W., Martin, R.L., Morokuma, K., Zakrzewski, V.G., Voth, G.A., Salvador, P., Dannenberg, J.J., Dapprich, S., Daniels, A.D., Farkas, O., Foresman, J.B., Ortiz, J. V., Cioslowski, J., Fox, D.J., 2009. Energy and Fuels. Gaussian Inc., Wallingford CT.
Gao, S., Khan, A., Nazari, M., Mirzaei, H., Ng Kay Lup, A., Baei, M.T., Chandiramouli, R., Soltani, A., Salehi, A., Javan, M., Jokar, M.H., Pishnamazi, M., Nouri, A., 2021. Molecular modeling and Simulation of glycine functionalized $B_{12}N_{12}$ and $B_{16}N_{16}$ nanoclusters as potential inhibitors of proinflammatory cytokines. J. Mol. Liq. 343, 117494.
Gao, Z., Zhi, C., Bando, Y., Golberg, D., Serizawa, T., 2011. Noncovalent functionalization of disentangled boron nitride nanotubes with flavin mononucleotides for strong and stable visible-light emission in aqueous solution. ACS Appl. Mater. Interfaces 3, 627–632.
Ghahremani, S., Samadizadeha, M., Khaleghian, M., Zabarjad Shiraz, N., 2019. Theoretical study of encapsulation of Floxuridine anticancer drug into BN (9,9–7) nanotube for medical application. Phosphorus, Sulfur, Silicon Related Elements, 293–306.
Grzybowska, K., Paluch, M., Wlodarczyk, P., Grzybowski, A., Kaminski, K., Hawelek, L., 2012. Enhancement of amorphous celecoxib stability by mixing it with octaacetylmaltose: the molecular dynamics study. Mol. Pharmaceutics 9, 894–904.
Gundersen, Grete, Rankin, D.W.H., 1983. Acta Chem. Scand. Part A 37, 865–874.
Gupta, P., Kakumanu, V.K., Bansal, A.K., 2004. Stability and solubility of celecoxib–PVP amorphous dispersions: a molecular perspective. Pharm. Res. 21, 1762–1769.
Haley, K.E., Almas, T., Shoar, S., Shaikh, S., Azhar, M., Habib Cheema, F., Hameed, A., 2021. The role of anti-inflammatory drugs and nanoparticle-based drug delivery models in the management of ischemia-induced heart failure. Biomed. Pharmacother. 142, 112014.
Half, E., Arber, N., 2009. Colon cancer: preventive agents and the present status of chemoprevention. Expert Opin. Pharmacother. 10 (2), 211–219.
He, C., Wang, J., Fu, L., Zhao, C., Huo, J., 2021. Associative vs. dissociative mechanism: electrocatalysis of nitric oxide to ammonia. Chin. Chem. Lett. https://doi.org/10.1016/j.cclet.2021.09.009.
Hesabi, M., Behjatmanesh-Ardakani, R., 2017. Interaction between anti-cancer drug hydroxycarbamide and boron nitride nanotube: A long-range corrected DFT study. Comput. Theor. Chem. 1117, 61–80.
Hezarkhani, S., Sedighi, S., Aghaei, M., Shamekhi, M., Nomali, M., 2014. Rheumatologic manifestations in Iranian patients with autoimmune thyroid diseases. J. Clin. Diagn. Res. 8, MC06–MC08.
Hoseininezhad-Namin, M.S., Pargolghasemi, P., Saadi, M., Ramezani Taghartapeh, M., Abdolahi, N., Soltani, A., Ng Kay Lup, A., 2020. Ab initio study of TEPA adsorption on pristine, Al and Si doped carbon and boron nitride nanotubes. J. Inorg. Organomet. Polym Mater. 30, 4297–4310.
Hu, L., Huang, X., Zhang, S., Chen, X., Dong, X., Jin, H., Jiang, Z., 2021. MoO.sub.3 structures transition from nanoflowers to nanorods and their sensing performances. J. Mater. Sci.: Mater. Electron. 32 (19), 23728.
Khalifi, M., Duverger, E., Gharbi, T., Boulahdour, H., Picaud, F., 2015. Theoretical demonstration of the potentiality of boron nitride nanotubes to encapsulate anticancer molecule. Phys. Chem. Chem. Phys. 17, 30057–30064.
Kim, O.T.P., Le, M.D., Trinh, H.X., Nong, H.V., 2016. In silico studies for the interaction of tumor necrosis factor-alpha (TNF-α) with different saponins from Vietnamese ginseng (Panax vietnamesis). Biophys. Physicobiol. 13, 173–180.
Lahiri, D., Rouzaud, F., Richard, T., Keshri, A.K., Bakshi, S.R., Kos, L., Agarwal, A., 2010. Boron nitride nanotube reinforced polylactide-polycaprolactone copolymer composite: mechanical properties and cytocompatibility with osteoblasts and macrophages in vitro. Acta Biomater. 6, 3524–3533.
Lee, H., Lee, J., 2013. J. Cryst. Growth 374, 37–42.
Li, X., Golberg, D., 2016. Boron nitride nanotubes as drug carriers. Boron Nitride Nanotubes Nanomed., 79–94
Li, Y., Macdonald, D.D., Yang, J., Qiu, J., Wang, S., 2020. Point defect model for the corrosion of steels in supercritical water: Part I, film growth kinetics. Corros. Sci. 163, 108280.
Li, H., Wang, F., 2021. Core-shell chitosan microsphere with antimicrobial and vascularized functions for promoting skin wound healing. Mater. Des. 204, 109683.
Li, X., Zhi, C., Hanagata, N., Yamaguchi, M., Bando, Y., Golberg, D., 2013. Boron nitride nanotubes functionalized with mesoporous silica for intracellular delivery of chemotherapy drugs. Chem. Commun. 49, 7337–7339.
Mlaouah, M., Tangour, B., El Khalifi, M., Gharbi, T., Picaud, F., 2018. The encapsulation of the gemcitabine anticancer drug into grapheme nest: a theoretical study. J. Mol. Model. 24, 102.
Moodley, I., 2008. Review of the cardiovascular safety of COXIBs compared to NSAIDS. Cardiovasc J Afr. 19 (2), 102–107.
Morris, G.M., Huey, R., Lindstrom, W., Sanner, M.F., Belew, R.K., Goodsell, D.S., Olson, A.J., 2009. AutoDock4 and AutoDockTools4: automated docking with selective receptor flexibility. J. Comput. Chem. 30 (16), 2785–2791.
Muñoz, A.D.O., Escobedo-Morales, A., Shakerzadeh, E., et al, 2021. Effect of homonuclear boron bonds in the adsorption of DNA nucleobases on boron nitride nanosheets. J. Mol. Liq. 322, 114951.
Nejati, K., Hosseinian, A., Vessally, E., Bekhradnia, A., Edjlali, L., 2017. A comparative DFT study on the interaction of cathinone drug with BN nanotubes, nanocages, and nanosheets. Appl. Surf. Sci. 422, 763–768.
Ocotitl Muñoz, A.D., Escobedo-Morales, A., Skakerzadeh, E., Chigo Anota, E., 2021. Effect of homonuclear boron bonds in the adsorption of DNA nucleobases on boron nitride nanosheets. J. Mol. Liq. 322, 114951.
Oh, L.M., 2006. Synthesis of celecoxib via 1,3-dipolar cycloaddition. Tetrahedron Lett. 47, 7943–7946.
Pakdel, A., Zhi, C., Bando, Y., Golberg, D., 2012. Low-dimensional boron nitride nanomaterials. Mater. Today 15, 256–265.
Pala, R., Pattnaik, S., Busi, S., Nauli, S.M., 2021. Nanomaterials as novel cardiovascular theranostics. Pharmaceutics 13, 348.
Palomino-Asencio, L., García-Hernandez, E., Salazar-Villanueva, M., Chigo-Anota, E., 2021. $B_{12}N_{12}$ nanocages with homonuclear bonds as a promising material in the removal/degradation of the insecticide imidacloprid. Physica E 126, 114456.
Parr, R.G., Szentpaly, L., Liu, S., 1999. J. Am. Chem. Soc. 121, 1922.
Parr, R.G., Yang, W., 1989. Density Functional Theory of Atoms and Molecules. Oxford University Press, New York.

Pavase, L.S., Mane, D.V., Baheti, K.G., 2018. Anti-inflammatory exploration of sulfonamide containing diaryl pyrazoles with promising COX-2 selectivity and enhanced gastric. J. Heterocycl. Chem. 00, 00.

Pease, R.S., 1952. An X-ray study of boron nitride. Acta Crystallogr. 5, 356.

Penning, T.D., Talley, J.J., Bertenshaw, S.R., Carter, J.S., Collins, P. W., Docter, S., Graneto, M.J., Lee, L.F., Malecha, J.W., Miyashiro, J.M., Rogers, R.S., Rogier, D.J., Yu, S.S., Anderson, G.D., Burton, E.G., Nita Cogburn, J., Gregory, S.A., Koboldt, C. M., Perkins, W.E., Seibert, K., Veenhuizen, A.W., Zhang, Y.Y., Isakson, P.C., 1997. Synthesis and biological evaluation of the 1,5-diarylpyrazole class of cyclooxygenase-2 inhibitors: identification of 4-[5-(4-methylphenyl)-3-(trifluoromethyl)-1H-pyrazol-1-yl]benzene sulfonamide (SC-58635, Celecoxib). J. Med. Chem. 40, 1347–1365.

Perdew, J.P., Burke, K., Ernzerhof, M., 1996. Generalized gradient approximation made simple. Phys. Rev. Lett. 77, 3865.

Permyakova, E.S., Sukhorukova, I.V., Yu, L., Konopatsky, A.S., Kovalskii, A.M., Matveev, A.T., Lebedev, O.I., Golberg, D.V., Manakhov, A.M., Shtansky, D.V., 2017. Synthesis and characterization of folate conjugated boron nitride nanocarriers for targeted drug delivery. J. Phys. Chem. C 121, 28096–28105.

Price, M.L.P., Jorgensen, W.L., 2001. Rationale for the observed COX-2/COX-1 selectivity of celecoxib from Monte Carlo simulations. Bioorg. Med. Chem. Lett. 11, 1541–1544.

Qian, L., Zheng, J., Wang, K., Tang, Y., Zhang, X., Zhang, H., Huang, F., Pei, Y., Jiang, Y., 2013. Biomaterials 34, 8968–8978.

Roosta, S., Majid Hashemianzadeh, S., Ketabi, S., 2016. Encapsulation of cisplatin as an anti-cancer drug into boron-nitride and carbon nanotubes: molecular simulation and free energy calculation. Mater. Sci. Eng., C 67, 98–103.

Roshande, G., Semnani, S., Fazel, A., Honarvar, M., Taziki, M., Sedaghat, S., Abdolahi, N., Ashaari, M., Poorabbasi, M., Hasanpour, S., Hosseini, S., Mansuri, S., Jahangirrad, A., Besharat, S., Moghaddami, A., Mirkarimi, H., Salamat, F., Ghasemi-Kebri, F., Jafari, N., Shokoohifar, N., Gholami, M., Sadjadi, A.K., Poustchi, H.K., Bray, F., Malekzadeh, R., 2018. Building cancer registries in a lower resource setting: the 10-year experience of Golestan, Northern Iran. Cancer Epidemiol. 52, 128–133.

Saikia, N., Deka, R.C., 2014. Density functional study on noncovalent functionalization of pyrazinamide chemotherapeutic with graphene and its prototypes. New J. Chem. 38, 1116–1128.

Saikia, N., Pandey, R., 2018. Polarity-induced surface recognition and self-assembly of noncanonical DNA nucleobases on h-BN monolayer. J. Phys. Chem. C 122, 3915–3925.

Saikia, N., Jhab, A.N., Deka, R.C., 2013. Interaction of pyrazinamide drug functionalized carbon and boron nitride nanotubes with pncA protein: a molecular dynamics and density functional approach. RSC Adv. 3, 15102–15107.

Schönthal, A.H., Chen, T.C., Hofman, F.M., Louie, S.G., Petasis, N. A., 2008. Celecoxib analogs that lack COX-2 inhibitory function: preclinical development of novel anticancer drugs. Expert Opin. Investig. Drugs 17 (2), 197–208.

Shayan, K., Nowroozi, A., 2018. Boron nitride nanotubes for delivery of 5-fluorouracil as anticancer drug: a theoretical study. Appl. Surf. Sci. 428, 500–513.

Singla, P., Riyaz, M., Singhal, S., Goel, N., 2016. Theoretical study of adsorption of amino acids on graphene and BN sheet in gas and aqueous phase including empirical DFT Dispersion correction. Phys. Chem. Chem. Phys. 18, 5597–5604.

Soltani, A., Baei, M.T., Tazikeh Lemeski, E., Pahlevani, A.A., 2014. The study of SCN^- adsorption on $B_{12}N_{12}$ and $B_{16}N_{16}$ nano-cages. Superlattices Microstruct. 75, 716–724.

Soltani, A., Baei, M.T., 2019. A DFT study on structure and electronic properties of BN nanostructures adsorbed with dopamine. Computation 7, 61.

Soltani, A., Bezi Javan, M., Hoseininezhad-Namin, M.S., Tajabor, N., Tazikeh Lemeski, E., Pourarian, F., 2017. Interaction of hydrogen with Pd- and co-decorated C24 fullerenes: density functional theory study. Synth. Met. 234, 1–8.

Soltani, A., Ramezanitaghartapeh, M., Bezi Javan, M., Baei, M.T., Ng Kay Lup, A., Mahon, P.J., Aghaei, M., 2020. Influence of the adsorption of toxic agents on the optical and electronic properties of $B_{12}N_{12}$ fullerene in the presence and absence of an external electric field. New J. Chem. 44, 14513–14528.

Soltani, A., Khan, A., Mirzaei, H., Onaq, M., Javan, M., Tavassoli, S., Mahmoodi, N.O., Arian Nia, A., Yahyazadeh, A., Salehi, A., Khandoozi, S.R., Masjedi, R.K., Rahman, M.L., Sarjadi, M.S., Sarkar, S.M., Su, C.-H., 2022. Improvement of anti-inflammatory and anticancer activities of poly(lactic-co-glycolic acid)-sulfasalazine microparticle via density functional theory, molecular docking and ADMET analysis. Arabian J. Chem. 15, 103464.

Srimathi, U., Nagarajan, V., Chandiramouli, R., 2018. Detection of nucleobases using 2D germanane nanosheet: a first-principles study. Comput. Theor. Chem. 1130, 68–76.

Srimathi, U., Nagarajan, V., Chandiramouli, R., 2018. Interaction of Imuran, Pentasa and Hyoscyamine drugs and solvent effects on graphdiyne nanotube as a drug delivery system - A DFT study. J. Mol. Liq. 265, 199–207.

Sukhorukova, I.V., Zhitnyak, I.Y., Kovalskii, A.M., Matveev, A.T., Lebedev, O.I., Li, X., Gloushankova, N.A., Golberg, D., Shtansky, D.V., 2015. Boron nitride nanoparticles with a petal-like surface as anticancer drug-delivery systems. CS Appl. Mater. Interfaces 31, 17217–17225.

Talla, J.A., Al-Khaza'leh, K.A., Ghozlan, A.A., 2019. Boron nitride nanotubes as a container for 5-fluorouracil anticancer drug molecules: molecular dynamics simulation study. Adv. Sci., Eng. Med. 11, 383–388.

Vessally, E., Salary, M., Arshadi, S., Hosseinian, A., Edjlali, L., 2018. The interaction of phosgene gas with different BN nanocones: DFT studies. Solid State Commun. 269, 23–27.

Vijayakumar, B., Kannappan, V., Sathyanarayanamoorthi, V., 2016. J. Mol. Struct. 1121, 16–25.

Vijayakumar, B., Kannappan, V., Sathyanarayanamoorthi, V., 2016. DFT analysis and spectral characteristics of Celecoxib a potent COX-2 inhibitor. J. Mol. Struct. 1121, 16–25.

Xu, S., Peng, H., Wang, N., Zhao, M., 2018. Inhibition of TNF-α and IL-1 by compounds from selected plants for rheumatoid arthritis therapy: In vivo and in silico studies. Trop. J. Pharm. Res. 17 (2), 277–285.

Xu, H., Wang, Q., Fan, G., Chu, X., 2018. Theoretical study of boron nitride nanotubes as drug delivery vehicles of some anticancer drugs. Theor. Chem. Acc. 104, 137.

Xu, H., Wang, Q., Fan, G., Chu, X., 2018. Theoretical study of boron nitride nanotubes as drug delivery vehicles of some anticancer drugs. Theor. Chem. Acc. 137, 104.

Xue, C., You, J., Zhang, H., Xiong, S., Yin, T., Huang, Q., 2021. Capacity of myofibrillar protein to adsorb characteristic fishy-odor compounds: effects of concentration, temperature, ionic strength, pH and yeast glucan addition. Food Chem. 363, 130304.

Zhang, L., Cong, M., Ding, X., Jin, Y., Xu, F., Wang, Y., Zhang, L., 2020. A Janus Fe-SnO2 catalyst that enables bifunctional electrochemical nitrogen fixation. Angew. Chem. (Int. Ed.) 59 (27), 10888–10893.

Zhang, Z., Ghosh, A., Connolly, P.J., Connolly, P.J., King, P., Wilde, T., Wang, J., Dong, Y., Li, X., Liao, D., Chen, H., Tian, G., Suarez, J., Bonnette, W.G., Pande, V., Diloreto, K.A., Shi, Y., Patel, S., Pietrak, B., Szewczuk, L., Sensenhauser, C., Dallas, S., Edwards, J.P., Bachman, K.E., Evans, D.C., 2021. J. Med. Chem. 64, 11570–11596.

Zhang, X., Tang, Y., Zhang, F., Lee, C., 2016. A novel aluminum-graphite dual-ion battery. Adv. Energy Mater. 6 (11), 1502588.

Zhang, H., Yamazaki, T., Zhib, C., Hanagata, N., 2012. Identification of a boron nitride nanosphere-binding peptide for the

intracellular delivery of CpG oligodeoxynucleotides. Nanoscale 4, 6343–6350.

Zhi, C., Bando, Y., Tang, C., Golberg, D., 2010. Boron nitride nanotubes. Mater. Sci. Eng. R 70, 92–111.

Zhu, J., Song, X., Lin, H.-P., Young, D.C., Yan, S., Marquez, V.E., Chen, C.-S., 2002. Using cyclooxygenase-2 inhibitors as molecular platforms to develop a new class of apoptosis-inducing agents. J. Natl. Cancer Inst. 94, 1745–1757.